INTERFEROMETRIC MAPPING OF MAGNETIC FIELDS IN STAR-FORMING REGIONS I. W51 E1/E2 MOLECULAR CORES

Shih-Ping Lai, Richard M. Crutcher, José M. Girart[1], and Ramprasad Rao[2]

Astronomy Department, University of Illinois, 1002 W. Green Street, Urbana, IL 61801;
slai@astro.uiuc.edu, crutcher@astro.uiuc.edu, jgirart@am.ub.es, ramp@oddjob.uchicago.edu

Draft version February 1, 2008

ABSTRACT

We present the first interferometric polarization map of the W51 e1/e2 molecular cores obtained with the BIMA array at 1.3 mm wavelength with approximately $3''$ resolution. The polarization angle varies smoothly across the double cores with an average position angle of $23°\pm5°$ for W51 e1 and $15°\pm7°$ for W51 e2. The inferred magnetic field direction is parallel to the minor axis of the double cores, which is consistent with the theoretical picture that clouds collapse along the field lines. However, the magnetic field may not determine the axis of angular momentum of these two cores as the field directions of the two cores significantly differ with the previously measured directions of rotational axes. The polarization percentage decreases toward regions with high intensity, suggesting that the dust alignment efficiency decreases toward high density regions. The field directions are highly ordered, and the small dispersion of the polarization angles implies that magnetic fields are strong ($\gtrsim 1$ mG) and perhaps dominate turbulence in W51 e1/e2.

Subject headings: ISM: magnetic fields – ISM: individual: W51 – polarization – star: formation – techniques: interferometric

1. INTRODUCTION

Star formation in molecular clouds is one of the most fundamental problems in astrophysics. It has become increasingly evident that star formation cannot be fully understood without considering magnetic fields (see recent reviews by Mouschovias & Ciolek 1999, and Shu et al. 1999). Magnetic fields provide explanations for the support of clouds against self-gravity, the formation and evolution of cloud cores, the origin of supersonic line widths, the low specific angular momentum of cloud cores and stars, and the formation of bipolar outflows. Unfortunately, the magnetic field remains the most poorly measured quantity in the star formation process. In order to advance our understanding of star formation, it is essential to improve our empirical knowledge of magnetic fields in molecular clouds.

The most promising technique to probe magnetic field morphology in dense molecular cores is to measure the linear polarization of the thermal emission from spinning, magnetically aligned dust grains (Heiles et al. 1993). Interstellar dust grains are elongated with their minor axes aligned with the magnetic field, thus the magnetic field direction in the plane of sky is perpendicular to the direction of polarization (Davis & Greenstein 1951; Roberge 1996). Millimeter interferometers detect the dust emission in the low optical depth regime with high angular resolution, thereby revealing the field morphology in the dense cores. In the past few years, linear polarization observations with the Berkeley-Illinois-Maryland Array (BIMA) of Orion-KL and NGC 1333 IRAS 4A have demonstrated the capability and reliability of polarization observations with this telescope (Rao et al. 1998; Girart et al. 1999). These results are not only consistent with the previous single-dish observations, but also provide new information at resolutions up to $3''$. Therefore, it is reasonable for us to carry out a large linear polarization survey of star-forming cores with BIMA.

W51 is a large molecular cloud/H II region complex at a distance of 7.0 ± 1.5 kpc (Genzel et al. 1981). Associated with ultracompact (UC) H II regions (Scott 1978), strong infrared and submillimeter continuum emission (Thronson & Harper 1979; Jaffe, Becklin, & Hildebrand 1984), molecular gas (Ho, Genzel, & Das 1983) and H_2O and OH masers (Genzel et al. 1981; Gaume & Mutel 1987), W51 is one of the most active high-mass star formation regions in our Galaxy. W51 e1 and W51 e2 are molecular cores located in the eastern edge of W51. The mass of W51 e1 and e2 are ~ 150 and $110\ M_\odot$, derived from NH_3 observations (Zhang & Ho 1997). With infall motions identified, these molecular cores are in the process of forming OB associations (Ho & Young 1996). Subarcsecond VLA observations reveal that W51 e1 contains three UC H II regions, e1, e3, e4 (Gaume, Johnston, & Wilson 1993), and a possibly dust source, e8 (Zhang & Ho 1997). In the vicinity of the UC H II region e2, there is a compact water maser concentration known as W51 Main (Genzel et al. 1981). Previous single-dish measurements with resolution $\sim30''$ show very low polarization in W51 e1/e2 consistent with non-detection (Kane et al. 1993; Dotson at al. 2000); however, this could be caused by averaging over the large beams. Our observations with 10 times better resolution will allow us to explore the field structure in the W51 e1/e2 cores.

In this paper, we present the first interferometric polarization map of the W51 e1/e2 cores at 1.3 millimeter wavelength. Other sources in our survey will be reported

---

[1] Current address: Departament d'Astronomia i Meteorologia, Universitat de Barcelona, 08028 Barcelona, Catalunya, Spain

[2] Current address: Department of Physics, University of Chicago

in later papers.

2. OBSERVATIONS AND DATA REDUCTION

Several observations were carried out from 1999 August to 2000 April using nine BIMA antennas with 1-mm SIS receivers and quarter-wave plates. The digital correlator was setup to observe the continuum emission with a 750 MHz window centered at 226.9 GHz in the lower sideband and a 700 MHz window centered at 230.9 GHz in the upper sideband. Strong CO J=2–1 line emission was isolated in an additional 50 MHz window in the upper sideband. The primary beam is $\sim 50''$ at 1.3 mm wavelength. Data were obtained in the B, C and D array configurations with projected baseline ranges from 6–170 kilowavelengths, resulting in a linear polarization map of the W51 e1/e2 cores with a long integration time, ~ 25 hours.

The BIMA polarimeter and the calibration procedure are described in detail by Rao et al. (in preparation). A pair of quarter-wave plates was placed in front of the linearly polarized receiver of each antenna in order to enable the detection of the left (L) and right (R) circularly polarized radiation. Four cross correlations, LL, RR, LR, and RL, must be measured at each baseline in order to obtain the four Stokes parameters, I, Q, U, and V (Thompson, Moran, & Swenson 1986). Because there was only one receiver at each BIMA antenna, the quarter-wave plates were switched on a time scale shorter than the uv-cell transit time to achieved quasi-simultaneous dual polarization observations. Walsh function switching patterns (Thompson, Moran, & Swenson 1986; Harmuth 1969) were used to maximize the efficiency of obtaining four cross correlations (Rao 1999). Sixteen switch patterns were needed to complete a cycle. The integration time of each pattern was set to 11.5 seconds and the plate switch took an additional 2–3 seconds; therefore, one cycle was about 4 minutes.

Calibration and data reduction were carried out using the MIRIAD software (Sault, Teuben, & Wright 1995). The instrumental polarization response ("leakage") was calibrated by observing the strongly polarized quasars 3C273 or 3C279 over a wide hour angle range, typically more than 5 hours. The observed polarization, including contributions from the instrumental polarization and the polarization of the calibrator, varied with hour angle due to the fact that the polarization vector of the calibrator rotates with respect to the linear feed horn. On the other hand, the instrumental polarization is constant with time. Therefore, the leakages can be solved by assuming that the polarization of the calibrator was constant in the frame of sky over the whole track. Task GPCAL of MIRIAD was used to solve simultaneously for the leakages and antenna gains from the polarization calibrator. The average leakage of each antenna was 5.9%±0.4% for our observations. The leakage correction of each antenna was applied to visibility data before further processing.

Channels with line emission were carefully flagged out in the visibility data of the continuum bands. As the continuum emission of the the W51 e1/e2 cores was stronger than the phase calibrator (QSO 1751+096), self-calibration was performed for refining antenna gain solutions. The Stokes I image was made with Briggs' robust weighting of 0.5 (Briggs 1995; Sault & Killeen 1998) to acquire a smaller beam size ($2''.7\times2''.0$, PA=1°) for better determination of

the self-calibration model. The model was used to calibrate the visibility data in order to obtain new gain solutions with shorter time intervals. The above iterations were repeated until the Stokes I image was not sufficiently improved. The Stokes Q and U images were then made with natural weighting to obtain the highest S/N ratio. The resulting synthesized beam was $3''.2\times2''.3$ with PA=2°. Maps of Stokes Q and U were deconvolved and binned to approximately half-beamwidth per pixel ($1''.5\times1''.2$) to reduce oversampling in our statistics. We then combined the maps to obtain the observed linearly polarized intensity,

$$I_{p,obs} = \sqrt{Q^2 + U^2}, \qquad (1)$$

and the polarization position angle,

$$\phi = 0.5 \; \tan^{-1}(U/Q). \qquad (2)$$

As the polarized intensity is an intrinsically positive quantity, Eq. (1) will tend to overestimate the polarized intensity. Therefore, a bias correction for the polarized intensity must be performed (Leahy 1989),

$$I_p = \sqrt{I_{p,obs}^2 - \sigma_{I_p}^2}, \qquad (3)$$

where the rms noise value of polarized intensity, σ_{I_p}, was taken as the average value of the rms noise in the Q and U maps, as the noise levels in these two maps are comparable. The polarization percentage was calculated from

$$p = \frac{I_p}{I}. \qquad (4)$$

The measurement uncertainty in the position angle,

$$\sigma_\phi = 0.5 \; \tan^{-1}(\sigma_{I_p}/I_p), \qquad (5)$$

depends on both σ_{I_p} and I_p, thus it varies across the map. When weighted with I_p, the average measurement uncertainty in the position angle for our observations was 5°.6±1°.7.

3. RESULTS AND ANALYSIS

Figure 1 displays a contour map of the 1.3-mm continuum from the W51 e1/e2 cores overlaid with polarization vectors. Polarization is called detected at positions where the linearly polarized intensity is greater than $3\sigma_{I_p}$ ($1\sigma_{I_p}$ = 4.7 mJy beam^{-1}) and the total intensity is greater than $5\sigma_I$ ($1\sigma_I = 27$ mJy beam^{-1}, which is dominated by incomplete deconvolution rather than thermal noise). Under these criteria, the polarized emission extends over an area of $\sim$12 beam sizes. Table 1 lists the polarization measurements in the W51 e1/e2 cores at selected positions, separated by approximately the synthesized beamsize. The distributions of the polarization angle and the polarization percentage are shown in Figure 2 and 3, respectively.

3.1. *Continuum and Polarized Emission*

The south and north continuum condensations of the double cores in Figure 1 correspond to W51 e1 and W51 e2, respectively. W51 e1 is extended (FWHM=$5''.0\times3''.0$, PA=11°) and its integrated flux is 8.2 Jy. W51 e2 is also resolved (FWHM=$4''.4\times3''.3$, PA=−8°) with an integrated flux of 13.6 Jy. We will refer to the intensity maxima of these two cores as "e1 1mm peak" and "e2 1mm peak". Analysis of the continuum flux at multiple wavelengths has shown that W51 e1 and W51 e2 contain both free-free

emission and dust emission (Rudolph et al. 1990). The expected flux of the free-free emission at 1.3 mm wavelength for these two cores can be estimated from their SEDs (Rudolph et al. 1990), which are ~ 0.5 Jy for both cores. Therefore, the average fractions of the free-free emission in W51 e1 and e2 are $\sim$6% and $\sim$4%.

The polarized emission does not show two distinct peaks associated with W51 e1 and e2, but it mainly arises from an extended region across the two cores. The peak of polarized intensity is at $1''\!.2$ south of e1 1mm peak (Table 1). There is also a compact region of polarized emission $\sim 4''$ northwest of e2 1mm peak (for convenience, we name this position "e2 pol NW"; cf. Fig. 1). The polarized flux drops to zero between e2 1mm peak and e2 pol NW, and e2 pol NW shows very different polarization angle. Therefore, the polarization in e2 pol NW may sample a different region, and is excluded in our statistical analysis.

Most of the polarized flux is associated with W51 e1. The elongated shape of W51 e1 is due to the fact that it is composed of emission from nearby UC H II regions (e1, e3 and e4), a newly discovered continuum source (e8: Zhang & Ho 1997), and the dust emission in the W51 e1 core. The nearest source to e1 1mm peak is e8, which indicates that e8 is stronger than the UC H II region e1 at 1.3 mm. Because the UC H II region e1 is stronger than e8 at 1.3 cm (Zhang & Ho 1997) and e8 is not detected at 2 cm (Gaume et al. 1993), the spectral index of e8 is very different from free-free emission. This fact is consistent with Zhang & Ho's suggestion that e8 is a dust-dominated continuum source. Hence, e8 is the most likely site for active star formation in the W51 e1 core.

The position of the UC H II region e2 (accurate to $0''\!.2$; Gaume et al. 1993) is offset $\sim 1''$ to northwest of e2 1mm peak . It is known that the molecular gas in W51 e2 is not evenly distributed around the H II region (Zhang & Ho 1997). If we consider that molecular gas is in general associated with dust grains, then, although the offset is small, it is evident that the free-free emission and the dust emission in W51 e2 do not coincide. Since the polarized intensity only originates from the dust emission and the fraction of the free-free emission could be significantly higher than the average value at the position of the UC H II region, this offset may be part of the reason for the absence of polarization between e2 1mm peak and e2 pol NW. It is interesting that the location of W51 Main is right in the polarization gap between e2 1mm peak and e2 pol NW, and a stream of water masers in W51 Main has been detected with proper motions headed toward position angle $200°$ (Leppänen, Liljeström, & Diamond 1998), which seems well matched with the direction of the polarization gap.

3.2. *Polarization Angle Distribution*

The polarization angle distribution in the W51 e1/e2 cores appears to be well matched to the morphology of the cores. Except that e2 pol NW has a very different position angle at $58°\pm8°$, the rest of the polarization vectors are uniformly distributed along the major axis of the double cores with an average position angle of $21°\pm6°$. Polarization vectors seem to be approximately parallel to local core edges: in W51 e1, polarization angles decrease westward and increase eastward from the central ridge to the edge; in W51 e2, position angles are close to $0°$ at the northeast edge; even for e2 pol NW, the difference between the polarization angle and the edge is less than $20°$. The polarization angles also follow the ridge connecting W51 e1 and W51 e2. Excluding e2 pol NW, we calculate the mean polarization angles for W51 e1 and W51 e2 weighted by the measurement uncertainty, which are $23°\pm5°$ for W51 e1 and $15°\pm7°$ for W51 e2. Compared to the measurement uncertainty, the variation of polarization angles corresponding to the core morphology is only slightly suggested by our data.

Figure 2 shows the distribution of the polarization angles in W51 e1 and W51 e2. The observed polarization angle dispersion $\delta\phi_{obs}$, defined to be the standard deviation of the position angles, is $4°\!.8\pm2°\!.0$ in W51 e1 and $6°\!.6\pm3°\!.0$ in W51 e2 (excluding e2 pol NW). Interestingly, these values are equal to the measurement uncertainty of the position angles σ_ϕ, $4°\!.9\pm1°\!.4$ in W51 e1 and $6°\!.7\pm3°\!.4$ in W51 e2. The observed dispersion is made up of contributions from the measurement uncertainty and the intrinsic dispersion $\delta\phi$, $\delta\phi_{obs}^2 = \delta\phi^2 + \sigma_\phi^2$, which indicates that the intrinsic dispersions in W51 e1 and e2 are very small. Therefore, if we take σ_ϕ as small as possible ($\sigma_\phi - 1\sigma_{\sigma_\phi}$) and $\delta\phi_{obs}$ as large as possible ($\delta\phi_{obs} + 1\sigma_{\delta\phi_{obs}}$), we can obtain the upper limit of the intrinsic dispersion, which is $5°\!.8$ in W51 e1 and $9°\!.0$ in W51 e2. Our results for the dispersion analysis are summarized in Table 2.

3.3. *Polarization Percentage Distribution*

The average polarization percentage of the W51 e1/e2 cores is $1.8\%\pm0.4\%$, including positions for which polarization vectors are not plotted in Fig. 1 because I_p is too small. W51 e2 has a lower polarization percentage ($1.1\%\pm0.3\%$) than that of W51 e1 ($3.2\%\pm0.6\%$). To better compare with previous observations, we convolved our map to $30''$ resolution with a Gaussian beam and obtained $1.3\%\pm0.2\%$ polarization with a position angle of $25°\pm3°$. The polarization detections we have obtained are clearly different from the single-dish results: at 1.3 mm (HPBW=$30''$), Kane et al. (1993) measured a polarization percentage of $0.50\%\pm0.21\%$ at an angle of $-31°\pm11°$; at $100\ \mu$m (HPBW=$35''$), Dotson at al. (2000) obtained zero polarization ($0.54\%\pm0.58\%$). However, all results could be still consistent, because the low S/N ratio of the these single-dish measurements can lead to large uncertainty in the polarization angle. Our observations demonstrate that high resolution is important for successful detection and mapping of magnetic fields in molecular cores.

Figure 3 shows plots of the polarization percentage versus Stokes I. These plots show that the polarization percentage decreases as the total intensity increases in both W51 e1 and W51 e2. Such a decrease in the polarization toward high intensity regions (*the depolarization*) has been commonly seen in polarization observations, e.g., L1755 (Lazarian, Goodman, & Myers 1997), OMC-1 (Schleuning 1998), and OMC-3 (Matthews & Wilson 2000). Lazarian, Goodman, & Myers (1997) have shown that the depolarization can be explained as a consequence of the dust alignment efficiency decreasing toward the inner parts of the dark clouds, as all known mechanisms of grain alignment fail under the typical physical conditions of dark cloud interiors. On the other hand, beam smearing over

small-scale field structure can also produce low polarization percentage (Rao et al. 1998); this can only be verified by observations with higher resolution.

Due to the apparent close anti-correlation of the polarization percentage and the total intensity in Figure 3, it is interesting to perform a least-squares linear fit on these two quantities. We obtain $\log_{10}(p) = (-1.52 \pm 0.01) - (0.63 \pm 0.07) \times \log_{10}(I)$ with a correlation coefficient of -0.91 in W51 e1, and $\log_{10}(p) = (-1.73 \pm 0.01) - (0.99 \pm 0.04) \times \log_{10}(I)$ with a correlation coefficient of -0.97 in W51 e2. However, due to the difficulty of excluding the free-free emission at every position, direct comparison between our results and the dust alignment mechanisms cannot be done. The tight correlations hint that the depolarization in the W51 e1/e2 cores is a gradual and global effect. Therefore, it is unlikely that the depolarization is entirely caused by a sudden change of the alignment mechanism in a local region, as was reported in Orion-KL (Rao et al. 1998).

4. DISCUSSION

4.1. *Magnetic Field Morphology*

The magnetic field direction inferred from the paramagnetic relaxation of grain alignment is perpendicular to the direction of the linear polarization of the dust emission (Davis & Greenstein 1951). Therefore, the average directions of the magnetic fields are $113°\pm5°$ in W51 e1 and $105°\pm7°$ in W51 e2 (excluding e2 pol NW). The field directions are approximately parallel to the minor axis of the two cores, suggesting that matter collapsed along the field lines to form the parent cloud of the double cores. The uniform field structure in the W51 e1/e2 cores also suggests that ionized gas in the UC H II regions does not have much interaction with the magnetic field, or the interaction only exists on a scale smaller than our synthesized beam.

Comparison between the field morphology and the rotational axes of W51 e1 and W51 e2 provides interesting implications for the relation between magnetic fields and core formation. Rotational motions have been observed toward these two cores by Zhang, Ho, & Ohashi (1998) from analysis of the velocity gradient of CH_3CN emission, and the derived rotational axis is at $66°\pm27°$ for e1 and at $20°\pm17°$ for e2. Clearly, the rotational axes and the magnetic field directions of these two cores do not align with each other. Although it has been suggested that protostellar disks may drag the field lines as they rotate (Holland et al. 1996), it may not be the case for these two cores. The field directions vary smoothly along the two cores. Thus, it is unlikely that two independent rotating cores that twist the field lines separately would produce a matched field morphology. Therefore, the smooth magnetic field structure is most likely associated with the common envelope of e1 and e2. Zhang, Ho, & Ohashi (1998) caution that the uncertainty in their analysis may be large. However, if the difference between the directions of rotational axes and magnetic fields is indeed significant, the magnetic field of the parent cloud seems to have had no effect in determining the axis of angular momentum of these two cores.

4.2. *Estimation of the Magnetic Field Strength*

Owing to the lack of understanding of the detailed mechanism of grain alignment, the magnetic field strength cannot be directly derived from linear polarization measurements of dust emission (Lazarian, Goodman, & Myers 1997). However, Chandrasekhar & Fermi (1953, hereafter CF) have proposed a method to estimate the field strength from the dispersion of polarization angles ($\delta\phi$) by assuming that the variation in polarization angles results from the perturbation of Alfvén waves on the field lines. In this case, the field strength projected in the plane of the sky (B_p) is given by

$$B_p = Q\sqrt{4\pi\bar{\rho}}\ \frac{\delta v_{los}}{\delta\phi}, \qquad (6)$$

where $\bar{\rho}$ is the average density, δv_{los} is the rms line-of-sight velocity, and Q is 1 for CF's derivation. Detailed studies show that the CF formula tends to overestimate the field strength. Q can be reduced by several factors, such as the inhomogeneity of clouds and the line-of-sight averaging (Zweibel 1990; Myers & Goodman 1991). Ostriker, Stone, & Gammie (2001) calculate the value of Q from their simulations of turbulent clouds, and suggest that the CF formula with $Q \approx 0.5$ can account for the complex magnetic field and density structure, and provide accurate estimates of the plane-of-sky field strength under strong field cases when $\delta\phi \leq 25°$. Since the angle dispersion we measured in the W51 e1/e2 is small ($\delta\phi < 9°$; §3.2), it is interesting to work out the field strength estimates with the modified CF formula.

However, the two other quantities, $\bar{\rho}$ and δv_{los}, needed to complete this exercise have uncertainties not smaller than that of $\delta\phi$. The density of the W51 e1/e2 cores varies with the physical components and scales, and we should use the average density obtained from the region that the observed polarization is associated with. Zhang & Ho (1997) measure the NH_3 emission in the infall regions of the cores and derive $n_{H_2} \sim 3 \times 10^6$ cm^{-3}, which is probably too high for our purpose because the polarized intensity in the W51 e1/e2 seems to originate in a more extended region. From spectral decomposition of the whole W51 A region (including W51 e1/e2 and W51 IRS 1), Sievers et al. (1991) show that W51 A consists of a 20 K cold dust component with $n_H \sim 5 \times 10^4$ cm^{-3} ($n_H = 2n_{H_2}$) and a 60 K warm dust component with $n_H \sim 10^6$ cm^{-3}. This provides a range for the density as W51 e1/e2 may contain a mixture of both components. Because the column density of the warm dust is $\sim$5 times more than that of the cold dust and W51 e1/e2 is the densest region in W51 A (Sievers et al. 1991), W51 e1/e2 is more likely to have a density close to 10^6 cm^{-3}. It is also difficult to decompose δv_{los} that is associated with Alfvénic motion from the molecular linewidths which are broadened by the complicated dynamics in W51 e1/e2, such as infall (3.5 km s^{-1}: Zhang et al. 1998), rotation ($\sim$4 km s^{-1}: Zhang & Ho 1997), and possible outflow activities. The linewidth of an optically thin NH_3 line measured in the envelope of e1 and e2 by Young, Keto, & Ho (1998), Δv=1.25 km s^{-1}, may contain little contamination from dynamical motions. Therefore, we adopt $\delta v_{los} = \Delta v/\sqrt{8\ln 2} = 0.53$ km s^{-1}.

Given the large uncertainty of the input parameters, we can only calculate the lower limits of B_p using the upper limits of the angle dispersions obtained in §3.2. The derived B_p for the density limits of W51 e1/e2 are listed in

Table 2. Our results show that the lowest value of B_p in W51 e1/e2 is just comparable to the typical magnetic field strengths measured in molecular cores with $n_{H_2} = 10^{5-6}$ cm^{-3} using the Zeeman effect ($\sim 500\mu$G: Crutcher 1999). Since this typical field strength provides crucial contribution in cloud evolution (Crutcher 1999), our results show that the magnetic energy is an important component in the energetics of the W51 e1/e2 envelope. It can be shown that the ratio of the turbulent to magnetic energy is simply proportional to the square of the angle dispersion (Lai et al. 2001, in preparation). The small angle dispersions we measured here imply that the magnetic field dominates the turbulent motion in the regions that emit polarized flux in the W51 e1/e2 molecular cores.

5. CONCLUSIONS

We have measured linear polarization of the thermal dust emission at 1.3 mm toward the W51 e1/e2 cores with the BIMA array. The conclusions of our observations are the following:

- The magnetic field is parallel to the minor axis of the W51 e1/e2 cores, consistent with the theoretical picture that cloud cores form due to gravitational contraction along field lines. However, the significant difference between the directions of magnetic field and rotational axes hints that the magnetic field of the parent cloud does not determine the axis of the angular momentum of these two cores.

- The polarization percentage decreases toward the high intensity regions. The tight anti-correlation between log p and log I in both W51 e1 and W51 e2 implies that depolarization is a global effect and may be caused by the decreasing dust alignment efficiency toward higher density regions.

- The small dispersion of the polarization angles in W51 e1/e2 suggests that the magnetic field is strong ($\gtrsim 1$ mG) and dominates turbulence in the regions where the polarized flux arises.

REFERENCES

Briggs, D. S. 1995, PhD dissertation (available at the website http://www.aoc.nrao.edu/ftp/dissertations/dbriggs/diss.html)
Chandrasekhar, S., & Fermi, E. 1953, ApJ, 118, 113 (CF)
Crutcher, R. M. 1999, ApJ, 520, 706
Davis, L., & Greenstein, J. L. 1951, ApJ, 114, 209
Dotson, J. L., Davidson, J., Dowell, C. D., Schleuning, D. A., & Hildebrand, R. H. 2000, ApJS, 128, 335
Gaume, R. A., & Mutel, R. L. 1987, ApJS, 65, 193
Gaume, R. A., Johnston, K. J., & Wilson, T. L. 1993, ApJ, 417, 645
Genzel, R. et al. 1981, ApJ, 247, 1039
Girart, J. M., Rao, R., & Crutcher, R. M. 1999, ApJ, 525, 109
Harmuth, H. F. 1969, IEEE Spectrum, 6, No. 11, 82
Heiles, C., Goodman, A. A., McKee, C. F., & Zweibel, E. G. 1993, in Protostars and Planets III, ed. M. Matthews, & E. Levy (Tuscon: University of Arizona Press), 279
Ho, P. T. P., Das, A., & Genzel, R. 1983, ApJ, 266, 596
Ho, P. T. P., & Young, L. M. 1996, ApJ, 472, 742
Holland, W. S., Greaves, J. S., Ward-Thompson, D., & Andre, P. 1996, A&A, 309, 267
Jaffe, D. T., Becklin, E. E., & Hildebrand, R. H. 1984, ApJ, 279, L51
Kane, B. D., Clemens, D. P., Barvainis, R., & Leach, R. W. 1993, ApJ, 411, 708
Lai, S.-P., Crutcher, R. M., Girart, J. M., & Rao, R. 2001, submitted to ApJ
Lazarian, A., Goodman, A. A., & Myers, P. C. 1997, ApJ, 490, 273
Leahy, P., VLA Scientific Memoranda No. 161
Leppänen, K., Liljeström, T., & Diamond, P. 1998, ApJ, 507, 909
Matthews, B. C. & Wilson, C. D. 2000, ApJ, 531, 868
Mouschovias, T. Ch. 1976, ApJ, 207, 141
Mouschovias, T. Ch., & Ciolek, G. E. 1999, in The Origin of Stars and Planetary Systems, eds. C. J. Lada & N. D. Kylafis (Kluwer Academic Press), 305
Myers, P. C., & Goodman, A. A. 1991, ApJ, 373, 509

Ostriker, E. C., Stone, J. M., & Gammie, C. F. 2001, ApJ, 546, 980
Rao, R., Crutcher, R. M., Plambeck, R. L., & Wright, M. C. H. 1998, ApJ, 502, L75
Rao, R. 1999, Ph.D. Dissertation, University of Illinois at Urbana-Champaign
Rao, R., Crutcher, R. M., Girart, J. M., Lai, S.-P., Wright, M. C. H., Plambeck, R. L., & Lugten, J. B. 2001, in preparation
Roberge, W. G. 1996, ASP Conf. Ser. 97: Polarimetry of the Interstellar Medium, 401
Rudolph, A., Welch, W. J., Palmer, P., & Dubrulle, B. 1990, ApJ, 363, 528
Sault, R. J., & Killeen, N. E. B. 1998, Miriad Users Guide (available at the website http://www.atnf.csiro.au/computing/software/miriad)
Sault, R. J., Teuben, P. J., & Wright, M. C. H. 1995, ASP Conf. Ser. 77: Astronomical Data Analysis Software and Systems IV, 4, 433
Schleuning, D. A. 1998, ApJ, 493, 811
Scott, P. F. 1978, MNRAS, 183, 435
Shu, F. H., Allen, A., Shang, H., Ostriker, E. C., & Li, Z. 1999, in The Origin of Stars and Planetary Systems, eds. C. J. Lada & N. D. Kylafis (Kluwer Academic Press),193
Sievers, A. W., Mezger, P. G., Kreysa, E., Haslam, C. G. T., Lemke, R., & Gordon, M. A. 1991, A&A, 251, 231
Thompson, A. R., Moran, J. M., & Swenson, G. W. 1986, Interferometry and Synthesis in Radio Astronomy (New York: Wiley)
Thronson, H. A. & Harper, D. A. 1979, ApJ, 230, 133
Welch, W. J., et al. 1996, PASP, 108, 93
Young, L. M., Keto, E., & Ho, P. T. P. 1998, ApJ, 507, 270
Zhang, Q., & Ho, P. T. P. 1997, ApJ, 488, 241
Zhang, Q., Ho, P. T. P., & Ohashi, N. 1998, ApJ, 494, 636
Zweibel, E. G. 1990, ApJ, 362, 545

TABLE 1
POLARIZATION MEASUREMENTS IN THE W51 e1/e2 REGIONS

Position ($''$,$''$)[a]	Stokes I (Jy beam^{-1})	Polarization Percentage(%)	Polarization Angle (°)	Note
(-6.3, 3.3)	0.25±0.03	6.4±2.0	58± 8	e2 pol NW
(-1.0, 2.0)	0.35±0.03	5.6±1.4	1± 7	e2
(-3.6, 0.6)	3.22±0.03	0.7±0.2	19± 6	e2 1mm peak
(-1.6, 0.3)	0.91±0.03	1.5±0.5	10±10	e2
(-1.6,-2.9)	0.32±0.03	7.9±1.6	16± 5	e2 south
(-3.9,-2.9)	0.74±0.03	3.1±0.6	9± 6	e2 south
(-2.0,-6.3)	0.37±0.03	6.5±1.4	19± 6	e1
(-4.2,-6.3)	1.79±0.03	2.1±0.3	29± 4	e1 1mm peak
(-4.2,-7.5)	1.45±0.03	3.0±0.3	28± 3	Peak of polarized flux
(-6.5,-7.5)	0.30±0.03	5.8±1.6	7± 8	e1
(-2.0,-9.5)	0.20±0.03	10.0±2.7	26± 7	e1
(-4.2,-9.5)	0.63±0.03	4.8±0.8	28± 4	e1
e1 average	–	3.2±0.6	23± 5	
e2 average	–	1.1±0.3	15± 7[b]	
total average	–	1.8±0.4	21± 6[b]	

[a]Offsets are measured with respect to the phase center: α_{2000}=19^{h}23^{m}44^s.2, δ_{2000}=14°30′33″.4.
[b]e2 pol NW is excluded.

TABLE 2
ESTIMATES OF MAGNETIC FIELD STRENGTHS IN THE PLANE OF THE SKY

Region	σ_ϕ(°)[a]	$\delta\phi_{obs}$(°)[b]	$\delta\phi$ (°)[c]	n_H (cm^{-3})[d]	B_p (mG)[e]
e1	4.9±1.4	4.8±2.0	< 5.8	5×10^4	> 0.3
				10^6	> 1.3
e2	6.7±3.4	6.6±3.0	< 9.0	5×10^4	> 0.2
				10^6	> 0.8

[a]The measurement uncertainty of the polarization angle
[b]The observed polarization angle dispersion
[c]The intrinsic polarization angle dispersion
[d]The number density of atomic hydrogen
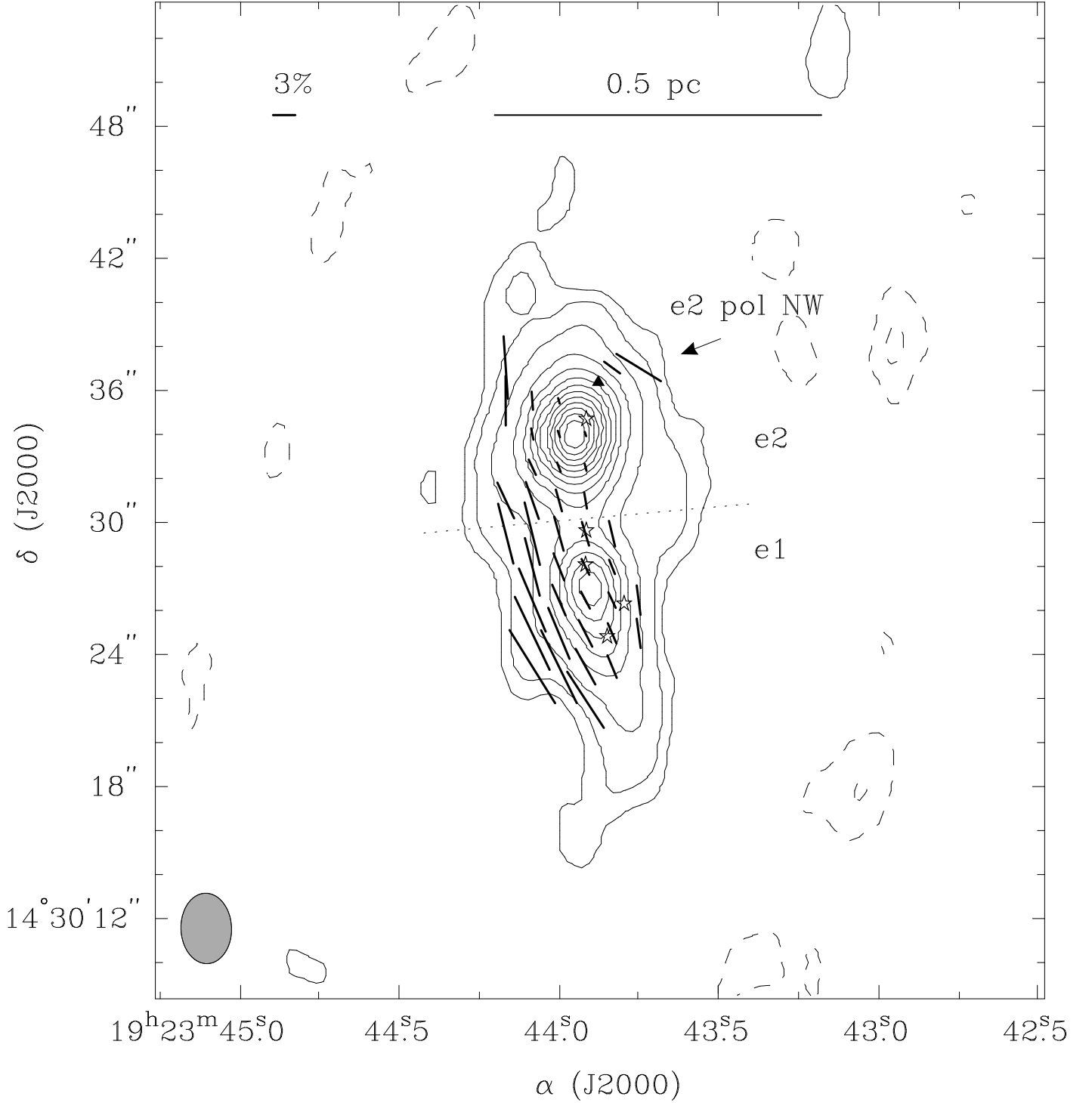[e]The plane-of-sky magnetic field strength

FIG. 1.— Polarization map of the W51 e1/e2 cores. The contours represent Stokes I at $-5, -3, 3, 5, 10, 20, 30, ..., 110$ σ levels. The 1 σ noise level of Stokes I is 27 mJy beam^{-1}. The line segments are polarization vectors, and their lengths are proportional to the polarization percentage with a scale of 3% per arcsec length. The dashed line that crosses the saddle point of the continuum is used to separate the data of W51 e1 and W51 e2 for our statistics. The star symbols mark the positions of e2, e4, e8, e1 and e3 from north to south. The triangle marks the position of H_2O masers near e2 (W51 Main). e2 pol NW refers to the two vectors northwest of W51 Main. The ellipse indicates the synthesized beam of the Stokes Q and U images, which is $3.''2 \times 2.''3$ with PA=$2°$. Positions with high intensity but without polarization detections may have higher fraction of free-free emission or/and have an environment inappropriate for the magnetic alignment of the dust grains.
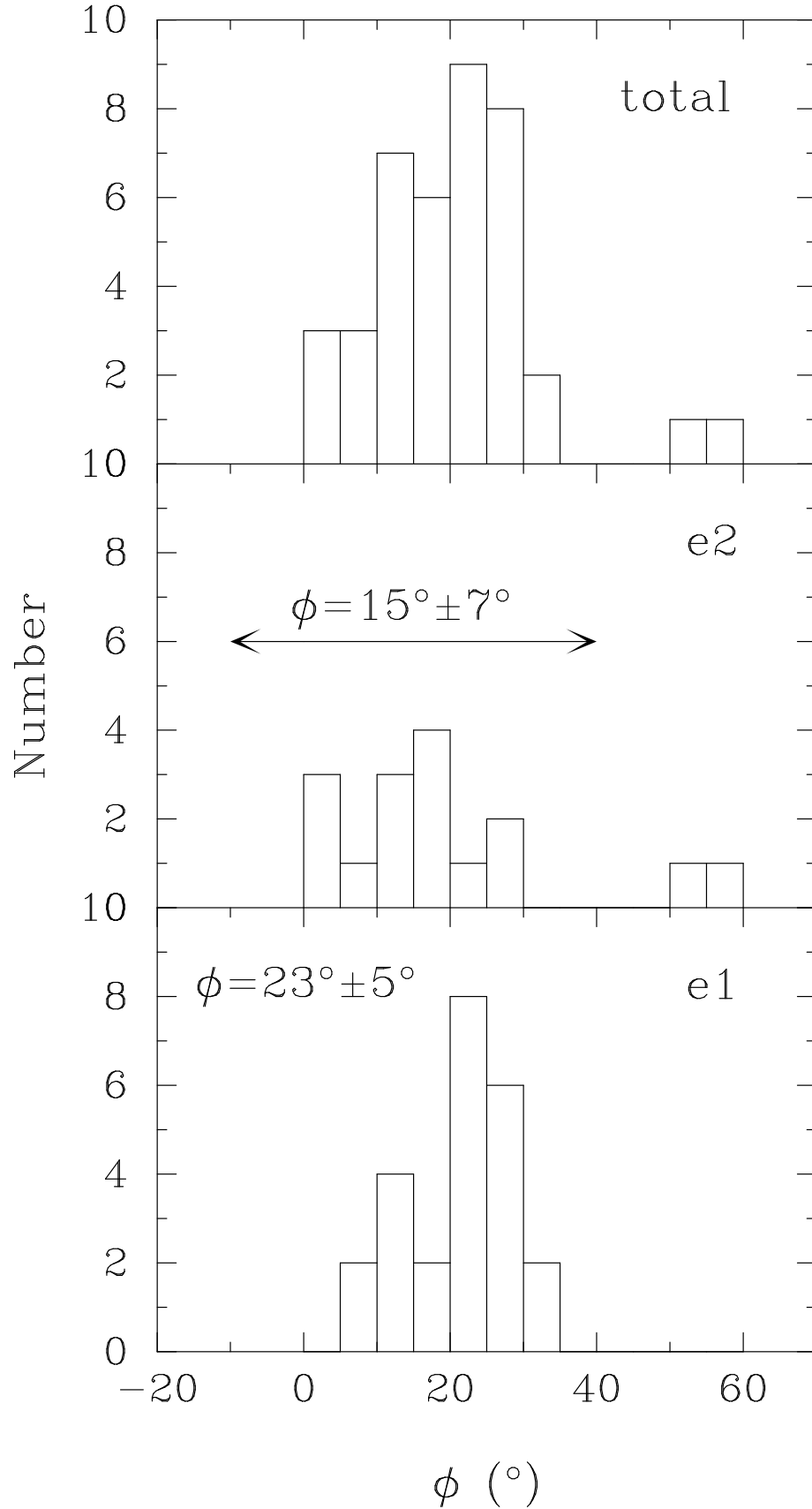
FIG. 2.— Distribution of polarization angle in W51 e1/e2. The average and the dispersion of the polarization angle in e1 and e2 are labeled, and the double arrow indicates that e2 pol NW with $\phi = 50° - 60°$ is excluded in the calculation.
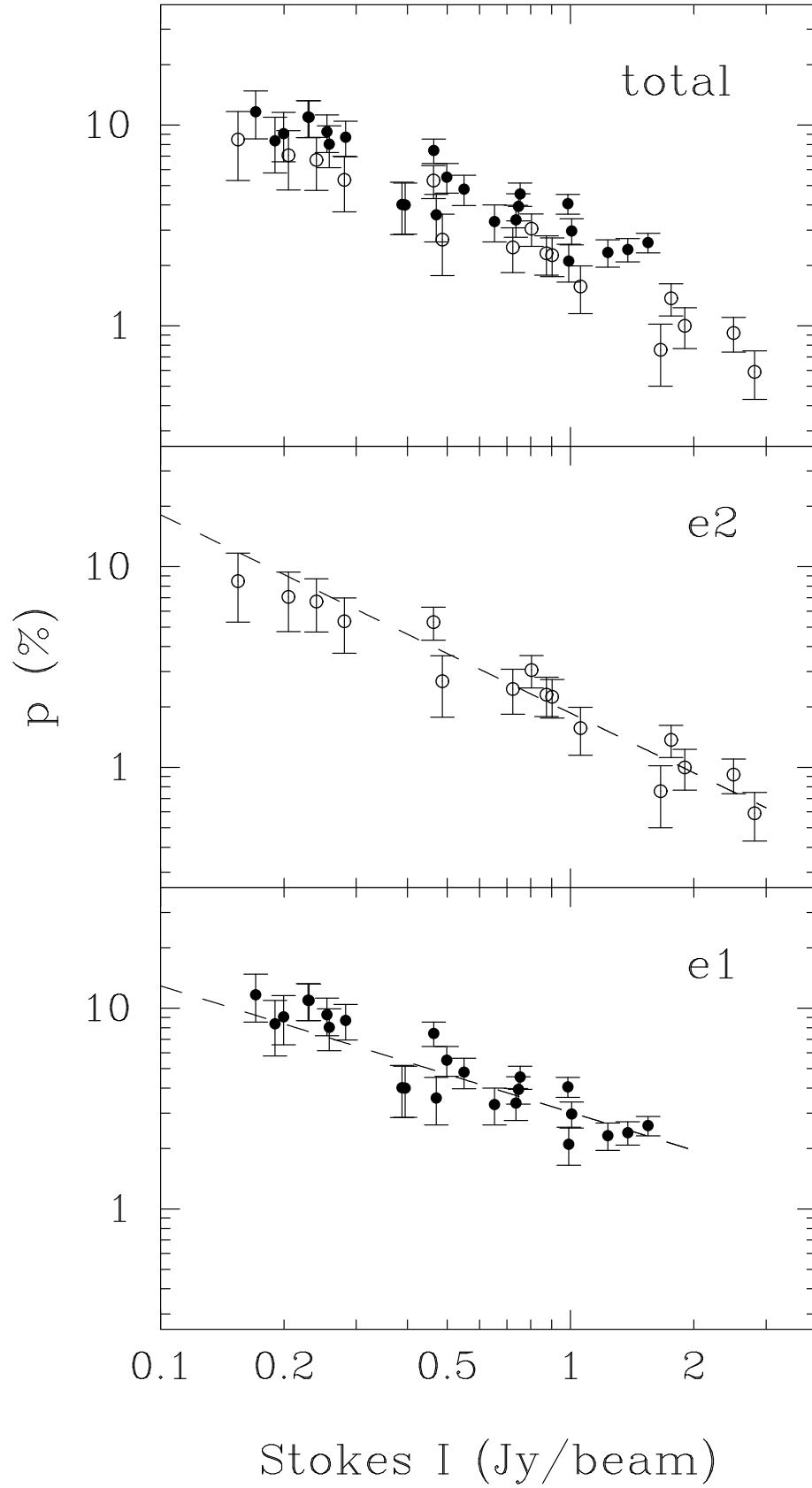
FIG. 3.— The variation of the polarization percentage with Stokes I in W51 e1/e2. The dashed lines are the results of the least-squares linear fit.